Pressurized N_2 directly fed to the $RuAu/CeO_{1.76}$ catalyst porous electrode in a proton exchange membrane electrolyzer favoring electrochemical NH_3 production

Lianqiao Tan,[a] Meng Wang,*[a] Mingming Deng,[a] Cheng Tong,[a] Xin Feng,[a] Qiang Liao,[b, c] Zidong Wei*[a]

a National-municipal Joint Engineering Laboratory for Chemical Process Intensification and Reaction, College of Chemistry and Chemical Engineering, Chongqing University, Chongqing, 400044, China

b Key Laboratory of Low-grade Energy Utilization Technologies and Systems, Ministry of Education, Chongqing 400030, China

c Institute of Engineering Thermophysics, School of Energy and Power Engineering, Chongqing University, Chongqing 400030, China

*E-Mail: zdwei@cqu.edu.cn; wmeng@cqu.edu.cn

Experimental Section

Materials: Cerium trichloride ($CeCl_3 \cdot 7H_2O$, AR), Sodium hydroxide (NaOH, AR), salicylic acid, sodium hydroxide, sodium citrate, sodium hypochlorite (NaClO, AR), sodium nitroprusside (AR), para-(dimethylamino) benzaldehyde (p-$C_9H_{11}NO$, AR), hydrochloric acid (HCl, AR), ethanol (AR), sulfanilic acid (AR), N-(1-naphthyl)-ethylenediamine dihydrochloride (AR), and acetic acid (AR) were purchased from Chuandong Chemical Group Co., Ltd., Chloroauric acid ($HAuCl_4$, AR), Ruthenium trichloride ($RuCl_3$, AR), and $(^{15}NH_4)_2SO_4$ (AR) were purchased from Aladdin Ltd. (Shanghai, China). Diluted water throughout all experiments was purified through a Millipore system.

Synthesis of $CeO_{1.80}$ and $CeO_{1.88}$ nanorods

The $CeO_2 \cdot xH_2O$ precursors were prepared through a typical hydrothermal method. Briefly, 1.48 g $CeCl_3 \cdot 7H_2O$ dissolved in 10 mL ultrapure H_2O was mixed with 19.2 g NaOH in 70 mL water under vigorous stirring for 2 h. Then the suspension solution was transferred into Teflon-lined autoclave, and kept in 100 ℃ for 24 h. After natural cool, the $CeO_2 \cdot xH_2O$ precursors were collected by centrifugation and washed by water and ethanol by three times, respectively, followed by vacuum-dried in 60.

For synthesis of $CeO_{1.80}$ nanorods, 300 mg of $CeO_2 \cdot xH_2O$ precursors were redispersed into 150 mL diluted H_2O under ultrasonic for 30 min, and then undergo a secondary hydrothermal treatment in 160 ℃ for 12 h. After cooling naturally, the $CeO_{1.80}$ nanorods were collected by centrifugation and washed by water and ethanol for three times, followed by vacuum-dried in 60 ℃.

For synthesis of CeO_2 nanorods with deficient oxygen vacancies, the $CeO_2 \cdot xH_2O$ powders were annealed at 700 ℃ for 4 h in muffle furnace. After cooling naturally, the obtained $CeO_{1.88}$ powders were mechanical ground and collected.

Synthesis of RuAu/$CeO_{1.76}$ and RuAu/$CeO_{1.84}$ hybrid catalysts

95 mg $CeO_{1.80}$ powders were uniformly dispersed in 20 mL dilute water under ultrasonic, and stirred in ice-water bath. A 5 mL mixture solution containing 3.3 mM $RuCl_3$ and 3.3 mM $HAuCl_4$ was added dropwise into the $CeO_{1.80}$ suspension. After continuous stirring for 3 h, the mixture was flash-frozen in liquid nitrogen, followed by lyophilized for 48 hours. 100 mg of the obtained $CeO_{1.80}$ supported RuAu precursors were transferred into a hermetically container under argon atmosphere. The container then underwent microwave irradiation for 15 s in microwave ovens with output power of 1000 W. After cooling naturally, the obtained black RuAu/$CeO_{1.76}$ powders were washed by

ethanol and water for three times, and vacuum-dried in sequence. The RuAu/$CeO_{1.84}$ were obtained as with the above methods, except for using $CeO_{1.88}$ as support.

Characterization

Transmission electron microscopy (TEM) images were detected on a FEI Tecnai G2 T20 microscope, and scanning transmission electron microscopy (STEM) measurements were conducted on a FEI Tecnai G2 F20 FEGTE microscope operated with electron acceleration energy of 200 kV. X-ray photoelectron spectra (XPS) analysis were performed on a Thermal ESCALAB 250 XI. The C 1s peak (284.8 eV) was employed as the reference standard. X-ray diffraction (XRD) data were recorded on a Shimadzu X-ray diffractometer, model 6000 at a scanning rate of 10 °C min−1. Electron paramagnetic resonance (EPR) spectra were recorded on X-band (νmw = 9.84 GHz) EMXmicro BRUKER spectrometer.

Electrochemical measurement in H-type cell

2 mg final powders and 2 mg commercial Carbon black was dispersed in the mixture containing 1.92 mL ethanol and 80 μL Nafion solution (5 %) under ultrasonic for 30 minutes. 250 μL of dispersed catalyst was deposited on hydrophobic carbon paper (1 cm^2) as the working electrode with catalyst loading mass of 0.25 mg cm^{-2}.

Before electrochemical test, the Nafion 117 membrane was pretreated by sequentially heating in H_2O2 solution (5 %) for 1 h, diluted H_2O for 1 h, 0.5 M H_2SO_4 solution for 1 h, and diluted H_2O for 1 h. The N_2 (99.999%) and Ar (99.999%) gas as feeding gas were purified by 100 mM NaOH, 50 mM $FeSO_4$, and 50 mM H_2SO_4 before flowing into the reaction system. The eNRR test was conducted in electrochemical workstation (660E) and a H-type cell separated by pretreated Nafion-

117 membrane using 0.5 M Li_2SO_4 solution as electrolyte filled in two compartments. The catalyst loaded on carbon paper, carbon rod, and saturated Ag/AgCl electrode severally served as working electrode, counter electrode, and reference electrode. The applied potentials against saturated Ag/AgCl reference electrode were iR-compensated and converted to the reversible hydrogen electrode (RHE) scale based on the following equation:

$$E_{(RHE)} = E_{(Ag/AgCl)} + 0.197\ V + 0.059 \times pH.$$

Electrochemical measurement in PEM cell

2 mg final powders and 2 mg commercial Carbon black was dispersed in the mixture containing 1.92 mL ethanol and 80 μL Nafion solution (5 %) under ultrasonic for 30 minutes. 2 mL dispersed catalyst was deposited on hydrophobic carbon paper (1 cm^2) as the eNRR electrode with catalyst loading mass of 2 mg cm^{-2}. 1 mg of commercial PtRu/C was dispersed in the mixture containing 0.96 mL of ethanol and 40 μL of Nafion solution (5 %) under ultrasonic for 30 minutes. 1 mL of the suspension was sprayed onto hydrophobic carbon paper (1 cm^2) as the HOR electrode with catalyst loading mass of 1 mg cm^{-2}. Before electrolysis, the N_2 flow was purified by NaOH, $FeSO_4$ and H_2SO_4 solution to eliminate the possible NH_3 and NO_x contaminations. After continuous ventilation for 10 min, CA tests were conducted at specified applied potentials for 10 min, and the outlet gas flow containing NH_3 production was bubbled into H_2SO_4 solution. After electrolysis, ventilation was continued for another 10 min to ensure the NH_3 production in N_2 flow was absorbed in H_2SO_4 solution.

Quantitative detection of NH_3 production in H-type cell

Indophenol blue method

For quantitative detection of NH_3 production in H-type cell after potentiostatic testing for 2 h,

2 mL electrolyte solution was subsequently mixed with 2 mL of 5 wt% salicylic acid solution containing 5 wt% sodium citrate and 1.0 M NaOH, 1 mL of 50 mM NaClO and 0.2 mL of 1 wt% sodium nitroferricyanide. After incubation for 2 h, the spectra with absorbance at 655 nm was measured using a UV-Vis spectrophotometer. According to the absorbance at 655 nm of standard $(NH_4)_2SO_4$ solution at various NH_3 concentrations in Li_2SO_4 solution, a calibration curve of concentration-absorbance (655 nm) was plotted for to accurately determine the NH_3 concentration.

IC method

To ensure the accuracy of results obtained from indophenol blue method, IC was additionally conducted, with the characteristic peaks of NH_4^+ centered at 6.1 min in the time-dependent spectra.

According to the area of the peak of standard $(NH_4)_2SO_4$ solution at various NH_3 concentrations, a linear equation correlating concentration with peak area was plotted for to accurately determine the concentration of NH_3 production.

NMR method

^{1}H-NMR measurements were additionally measured to trace the N-source of NH_3 production and further determine the concentration. In detail, after electrolysis using purified $^{14}N_2$ or $^{15}N_2$ (99.999%) gas as feeding gas, 5 mL of the H_2SO_4 solution containing NH_3 production was concentrated to 1 mL with the pH in the range of 1~2. After adding100 μL of D_2O into 900 μL of obtained solution, the NH_3 production was quantified, with the 1H NMR signal recorded on a Bruker 400 MHz system.

Quantitative detection of NH_3 production in PEM electrolyzer

The NH_3 generated in PEM electrolyzer was absorbed in H_2SO_4 solution (pH = 3), and quantitatively determined using the salicylate method. Typically, 2 mL the H_2SO_4 solution containing NH_3 production was diluted to 8 mL and sequentially mixed with 1 mL of 0.4 M salicylic sodium solution containing 0.32 M NaOH, 100 μL of NaClO solution (ρCl = 4 ~ 4.9) and NaOH (0.75 M), and 100 μL 1 wt% sodium nitroferricyanide for 1 h. The spectra with absorbance at 655 nm was measured using a UV-Vis spectrophotometer, and the concentration-absorbance curve was calibrated using standard $(NH_4)_2SO_4$ solutions for quantification of NH_3 production.

Calculations of NH_3 yield and Faradaic efficiency (FE):

The FEs for NH_3 generation was calculated by the following equation (1):

$$FE = \frac{3F \times C_{NH_3} \times V}{17 \times Q}$$

and rates for NH_3 generation was calculated by the following equation (2):

$$NH_3\ yield\ rate = \frac{C_{NH_3} \times V}{m \times t}$$

Where F is Faraday constant (96485 C mol^{-1}); C_{NH_3} is the measured mass concentration of NH_3 in the aqueous solution; V represents the volume of the reaction solution; Q is the quantity of electric charge achieved by integrating the i-t curve; m is the mass of catalyst loaded on the electrode support; t represents the time for potentiostatic testing.

Detection of N_2H_4 by-production.

The concentration of N_2H_4 in electrolyte solution after electrolysis for 2 h was determined by

Watt and Chrisp's method. Typically, 5.99 g of para-(dimenthylamino) benzaldehyde was dissolved in 300 mL of ethanol and 30 mL of concentrated HCl solution, which served as chromogenic agent. Then 5 mL of electrolyte solution after electrolysis was added to 5 mL of the above mixture, and incubated for 15 min. The spectra with absorbance at 455 nm was measured using a UV-Vis spectrophotometer, and the concentration-absorbance curve was calibrated using standard hydrazine hydrate solutions with a series of concentration in 0.5 M Li_2SO_4 solution for quantification of N_2H_4 by-production.

Determination of NO_2^- contamination.

The N-(-1-naphthyl)-ethylenediamine dihydrochloride spectrophotometric method was employed for determination of NO_2^- contamination. Typically, 0.5 g of sulfanilic acid and 5 mg of N-(1-naphthyl)-ethylenediamine dihydrochloride was dissolved in 90 mL of diluted water and 5 mL of acetic acid, followed by adjusting the volume to 100 mL with deionized water. The obtained solution as chromogenic agent was severally mixed with the blank and N_2-saturated electrolyte solution with volume ratio of 1:4. After incubation for 30 min, the absorption spectrum at 548 nm was measured using an UV-vis spectrophotometer.

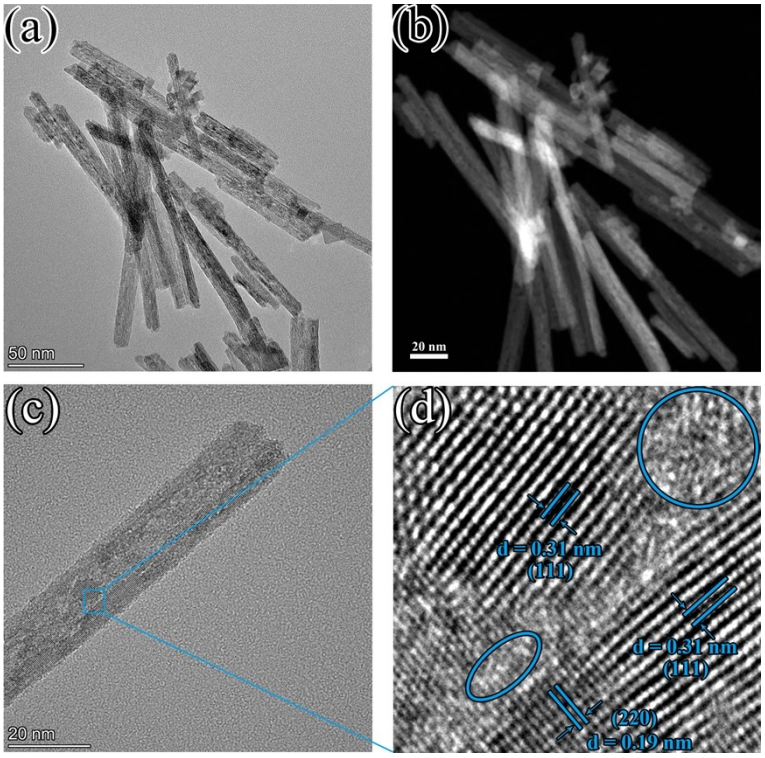

Figure S1. TEM images (a) and (c), HADDF-STEM image (b), and HRTEM (d) of RuAu/$CeO_{1.76}$ nanorods.

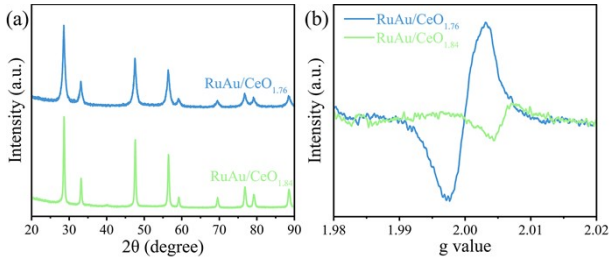

Figure S2. XRD patterns (a) and EPR spectra (b) of RuAu/$CeO_{1.76}$ and RuAu/$CeO_{1.84}$ nanorods.

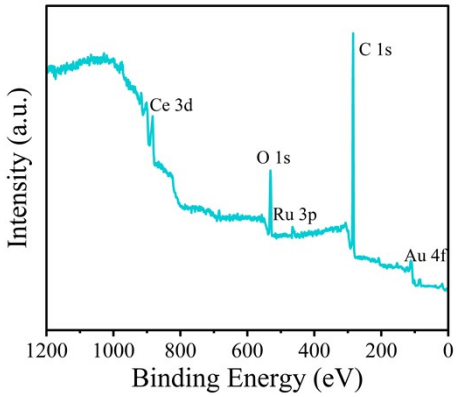

Figure S3. The Survey XPS spectrum of RuAu/$CeO_{1.76}$ catalyst displayed Ce and O with the presence of Ru and Au elements.

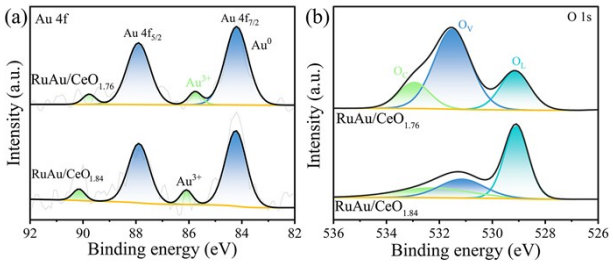

Figure S4. The high-resolution Au 4f (a) and O1s (b) XPS spectra of RuAu/$CeO_{1.76}$ catalyst. Particularly, oxygen vacancies in the metal oxides could bind with the H_2O molecules, and further decomposed into the OH- according to:

$$MO_{2-\delta} + H_2O \rightarrow MO_{2-\delta}\text{–}OH^* + H^+ + e^-,$$ [18]

That means the observed peak assigned to OV in the XPS spectra overlaps with the peak assigned to the OH-.

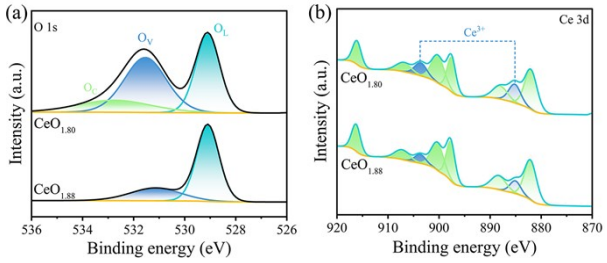

Figure S5. High-resolution O 1s (a) and Ce 3d (b) XPS spectra of pristine $CeO_{1.80}$ and $CeO_{1.88}$, respectively. In contrast, the O 1s (Fig. S5a,) and Ce 3d (Fig. S5b,) XPS spectra of pristine $CeO_{1.80}$ and $CeO_{1.88}$ were also recorded, achieving a limited percent of OVs and Ce^{3+} on the pristine supports. That is, the deposition of RuAu species further increased the concentration of surface OVs of the associated $CeO_{1.88}$ supports, which originated from the charge transfer from the supports to the RuAu species.

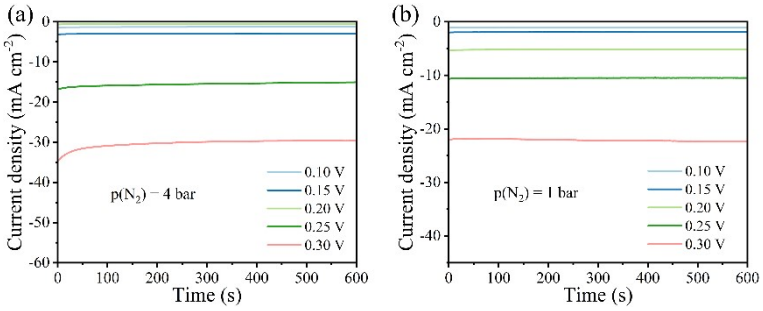

Figure S6. Chronoamperometry curves of RuAu/$CeO_{1.84}$ catalyst recorded at various potentials in PEM electrolyzer for 10 min with applied N_2 pressure of 4 bar (a) and 1 bar (b), which displayed the corresponding chronoamperometry

(CA) curves, with a negligible loss in current density.

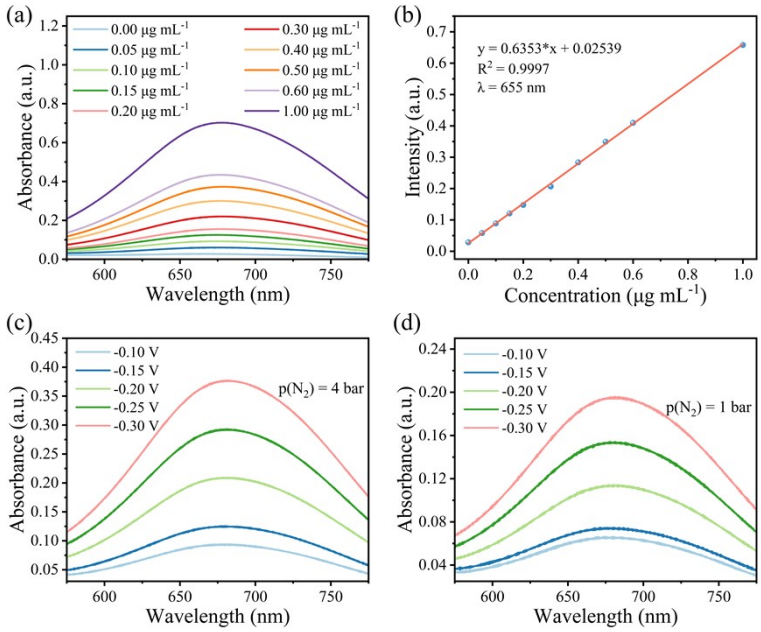

Figure S7. After electrolysis, the NH_3 production in the gas flow outlet the electrolyzer was absorbed in 30 ml of H_2SO_4 solution (pH=3), and then quantified by salicylic acid method combined with ultraviolet-visible spectroscopy. (a) UV-vis absorption spectra of $(NH_4)_2SO_4$ with different concentrations in H_2SO_4 solution (pH = 3). (b) The calibration curve for determination of NH_4^+ concentration. UV-vis absorption spectra of NH_3 production in H_2SO_4 solution (pH = 3) after eNRR in PEM electrolyzer under various cell voltage with applied N_2 pressure of 4 bar (c) and 1 bar (d).

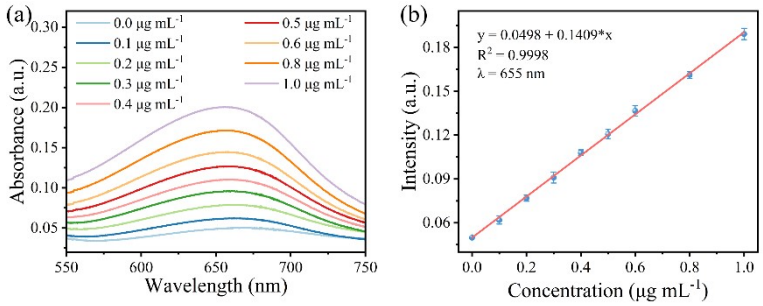

Figure S8. Using Indophenol blue method for quantitative detection of NH_4^+ after eNRR in 0.5 M Li_2SO_4 electrolyte solution. (a) UV-vis absorption spectra of $(NH_4)_2SO_4$ with different concentrations in 0.5 M Li_2SO_4 solution. (b)

The calibration curve for determination of NH_4^+ concentration (error bar = SD, n=3).

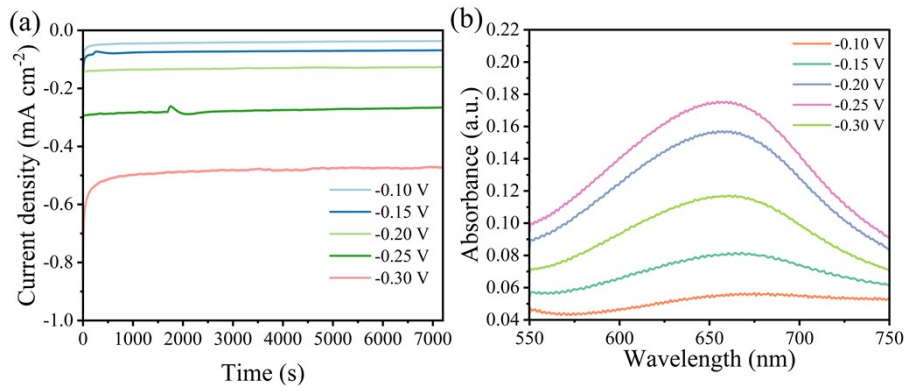

Figure S9. UV-vis absorption spectra of NH_4 production in 0.5 M Li_2SO_4 electrolyte after electrolysis for 2h under various applied potentials using RuAu/$CeO_{1.76}$ catalyst.

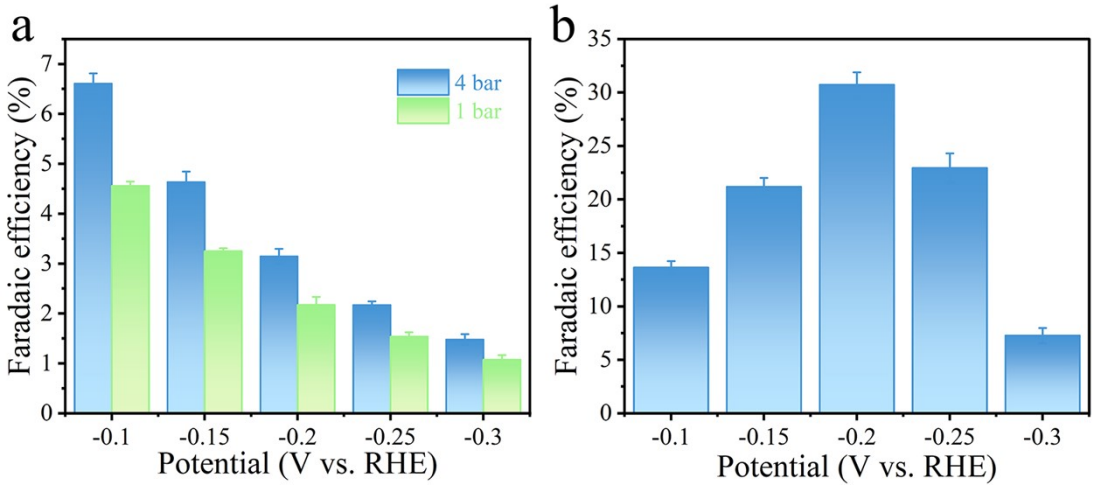

Figure S10. FE for NH_3 production using RuAu/$CeO_{1.76}$ catalyst various applied potentials (a) in PEM electrolyzer with N_2 pressure of 4 bar and 1 bar, respectively, and (b) in 0.5 M Li_2SO_4 electrolyte in H-type cell. However, the RuAu/$CeO_{1.76}$ catalyst displayed lower FEs in the PEM electrolyzer compared to those in the H-type cell, for significantly accelerated H^+ transfer kinetics in the PEM electrolyzer under higher current density preferentially enhanced the competitive HER process.

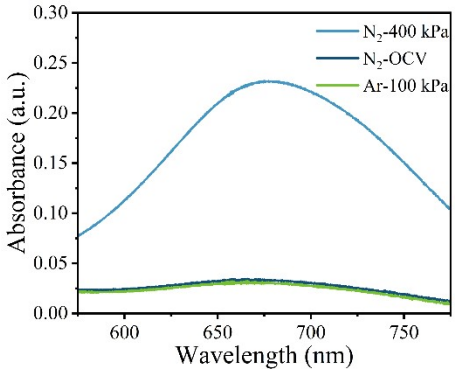

Figure S11. UV-vis absorption spectra of NH_3 production in H_2SO_4 solution after electrolysis in PEM electrolyzer coupled with RuAu/$CeO_{1.76}$-based GDE, with applied N_2 pressure of 4 bar under -0.3 V vs. RHE and OCV, and applied Ar pressure of 1 bar under -0.3 V vs. RHE, respectively. The interference of NH_3 contaminants in the H_2SO_4 solution and the feeding gas was excluded, further verifying the accuracy of the reaction results in the PEM electrolyzer.

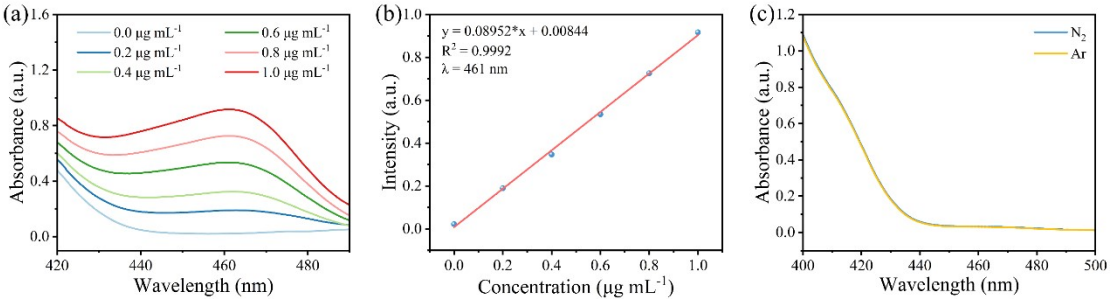

Figure S12. Using Watt and Chrisp's method for quantitative detection of N_2H_4 by-products in 0.5M Li_2SO_4 electrolyte solution. (a) UV-vis absorption spectra of N_2H_4 with different concentrations in 0.5 M Li_2SO_4 solution. (b) The calibration curve for quantitative determination of N_2H_4. (c) UV-vis absorption spectra of N_2H_4 in N_2- and Ar-saturated electrolyte after electrolysis. No N_2H_4 by-product was detected *via* Watt and Chrisp's method (Fig. S12), illustrating the high selectivity for electrochemical N_2-to-NH_3 conversion.

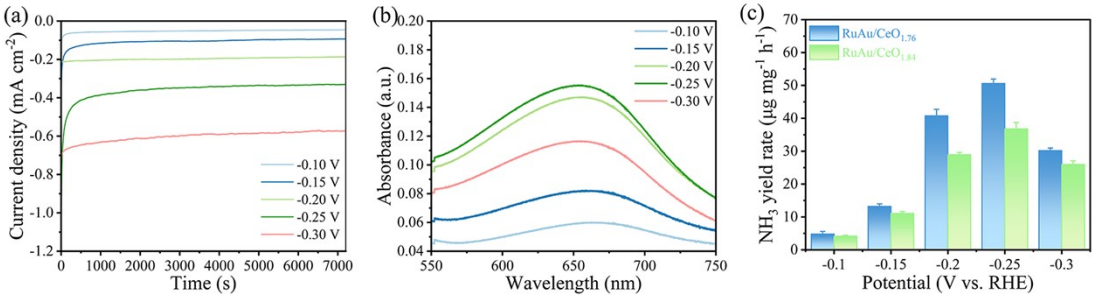

Figure S13. (a) Chronoamperometry curves of RuAu/$CeO_{1.84}$ catalyst recorded at various potentials in N_2-bubbled 0.5 M Li_2SO_4 solution for 2 h. (b) Corresponding UV-vis absorption spectra of NH_4+ production using RuAu/$CeO_{1.84}$ catalyst. (c) NH_3 generation rates of RuAu/$CeO_{1.76}$ and RuAu/$CeO_{1.84}$ at each given potential (error bar = SD, n=3).

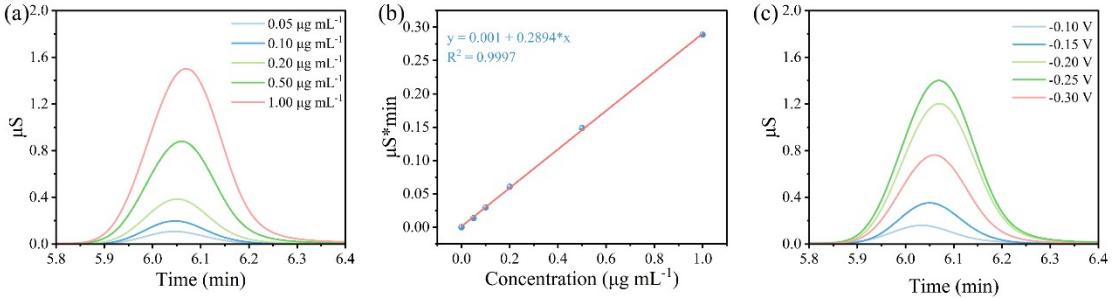

Figure S14. Using IC for detection and quantification of NH_4+ products after eNRR. (a) IC curves of standard NH_4+ solution with different concentrations in 0.5 M Li_2SO_4 solution. (b) The calibration curve for quantitative determination of NH_4^+. (c) IC curves of NH_3 production in electrolyte after electrolysis for 2h under various applied potentials using RuAu/$CeO_{1.76}$ catalyst.

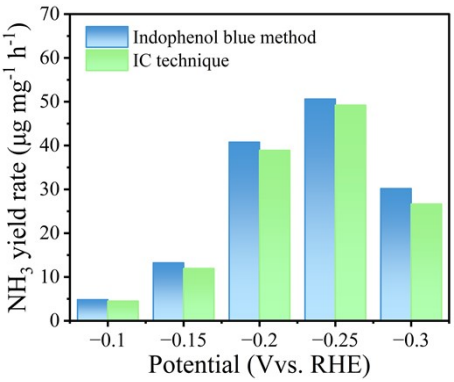

Figure S15. NH_3 production rates over RuAu/$CeO_{1.76}$ determined by IC technique and indophenol blue method. The NH_3 yield rates determined by ion chromatography (IC) fitted well with the results from the indophenol blue technique (Fig. S14 and S15), ensuring the accuracy of the eNRR performance.

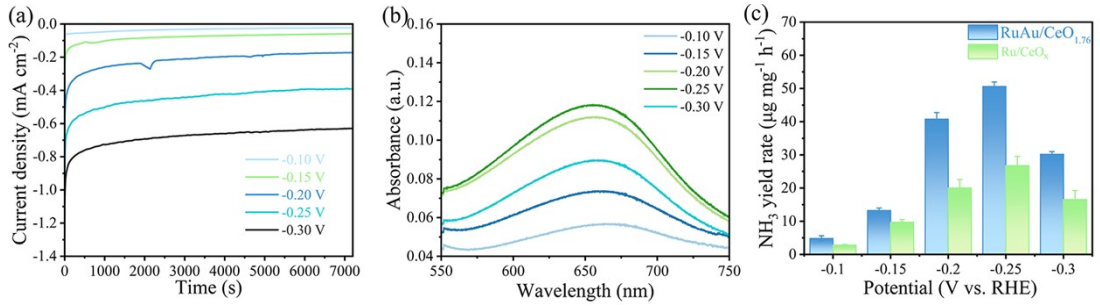

Figure S16. eNRR behavior of $Ru/CeO_{1.76}$ catalyst. (a) Chronoamperometry curves of Ru/CeO_2-VO catalyst recorded at various potentials in N_2-bubbled 0.5 M Li_2SO_4 solution for 2 h. (b) Corresponding UV-vis absorption spectra of NH_3 production using $Ru/CeO_{1.76}$ catalyst. FEs (c) and rates (d) for NH_3 generation of $RuAu/CeO_{1.76}$ and $Ru/CeO_{1.76}$ at each given potential (error bar = SD, n=3).

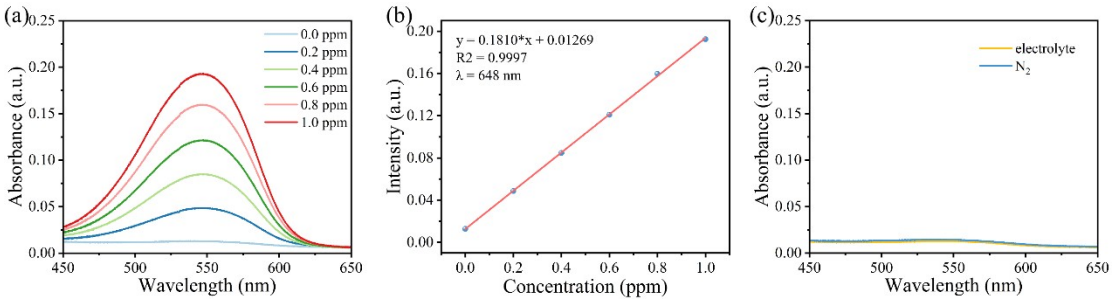

Figure S17. Using indophenol blue method for quantitative detection of NO_2^- contaminates in 0.5 M Li_2SO_4 electrolyte solution. (a) UV-vis absorption spectra of $NaNO_2$ with different concentrations in 0.5 M Li_2SO_4 solution. (b) The calibration curve for quantitative determination of NO_2^- contaminates. (c) UV-vis absorption spectra of NO_2^- in blank electrolyte and N_2-saturated electrolyte.

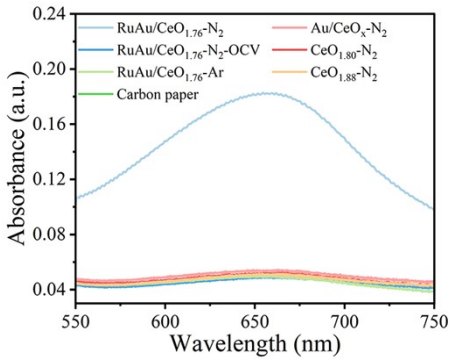

Figure S18. UV-vis absorption spectra of NH_4+ production in N_2-saturated 0.5 M Li_2SO_4 electrolyte after electrolysis at -0.25 V vs. RHE and OCV, and Ar-saturated electrolyte after electrolysis at -0.25 V using RuAu/$CeO_{1.76}$, and N_2-saturated electrolyte after electrolysis at -0.25 V vs. RHE using Au/CeO_x, $CeO_{1.80}$, $CeO_{1.88}$ and pristine carbon paper as electrodes, respectively. We additionally eliminated the influence of NOx pollutants in the primary electrolyte, and excluded the possible false positives from the N-containing pollution.

Table S1. The mass loading of Ru and Au in RuAu/$CeO_{1.76}$ and RuAu/$CeO_{1.84}$, respectively.

	RuAu/$CeO_{1.76}$	RuAu/$CeO_{1.84}$
Ru	1.652 %	1.636 %
Au	3.187 %	3.143 %

Table S2. Peak area percentage recorded from the XPS spectra.

Sample	**Peak area percentage (%)**			
	Ru^0	Au^0	Ce^{3+}	O_V
RuAu/$CeO_{1.76}$	72.23	98.31	24.47	59.77

$RuAu/CeO_{1.84}$	63.76	92.24	15.68	25.50
$CeO_{1.80}$			19.86	45.43
$CeO_{1.88}$			11.84	18.79

Table S3 Comparison of ENRR activity between $RuAu/CeO_{1.76}$ and other reported catalysts

Catalyst	Potential/voltage	Rates	Electrolyzer	Reference
$RuAu/CeO_{1.76}$	-0.3 V vs. RHE	30.17 μg mg-1 h-1	H-type cell	This work
	-0.3 V	185.53 μg mg^{-1} h^{-1}	PEM electrolyzer	
Mn-N_4/PC	-0.35 V vs. RHE	66.41 μg mg^{-1} h^{-1}	H-type cell	1
s-TiO_2 NTs	-0.6 V vs. RHE	16.67 μg mg^{-1} h^{-1}	H-type cell	2
PdCu/NC	-0.45 V vs. RHE	69.2 μg mg^{-1} h^{-1}	H-type cell	3
MXene/TiFeOx-700	-0.2 V vs. RHE	21.9 μg mg^{-1} h^{-1}	H-type cell	4
np-B	-0.4 V vs. RHE	23.11μg mg^{-1} h^{-1}	H-type cell	5
FePcTa-PPy	-0.2 V vs. RHE	31.47 μg mg^{-1} h^{-1}	H-type cell	6
Au–Fe_3O_4	-0.20 V vs. RHE	21.42 μg mg^{-1} h^{-1}	H-type cell	7
NiTe-800	-0.10 V vs. RHE	33.34 μg mg^{-1} h^{-1}	H-type cell	8
Fe1Sx@TiO_2	-0.20 V vs. RHE	18.3 μg mg^{-1} h^{-1}	H-type cell	9
Cu–TiO2	-0.55 V vs. RHE	21.31μg mg^{-1} h^{-1}	H-type cell	10
$Pd_{0.2}Cu_{0.8}$/rGO	-0.2 V vs. RHE	2.8 μg mg^{-1} h^{-1}	H-type cell	11
SA Ru-Mo_2CTX	-0.3 V vs. RHE	40.57 μg mg^{-1} h^{-1}	H-type cell	12
FeOOH QDs-GS	-0.4 V vs. RHE	27.3 μg mg^{-1} h^{-1}	H-type cell	13

Mo(IV)-Doped FeS_2	-0. V vs. RHE	25.15 μg mg^{-1} h^{-1}	H-type cell	14
Cu-coated GDE	-0.5 V vs. RHE	2.14 nmol cm^{-2} s-1	Flow reactor	15
SACs-MoS_2-Fe	-0.2 V vs. RHE	36.1 mmol g^{-1} h^{-1}	Flow reactor	16
Ru/CB	-0.1 V vs. RHE	0.99 nmol cm^{-2} s-1	Flow reactor	17

Reference

1. L. Han, M. Hou, P. Ou, H. Cheng, Z. Ren, Z. Liang, J. A. Boscoboinik, A. Hunt, I. Waluyo, S. Zhang, L. Zhuo, J. Song, X. Liu, J. Luo, and H. Xin, *ACS Catalysis*, 2020, 11, 509-516.
2. P. Li, Z. Jin, Z. Fang and G. Yu, *Angew. Chem. Int. Ed. Engl.*, 2020, **59**, 22610-22616.
3. L. Han, Z. Ren, P. Ou, H. Cheng, N. Rui, L. Lin, X. Liu, L. Zhuo, J. Song, J. Sun, J. Luo and H. L. Xin, *Angew. Chem. Int. Ed. Engl.*, 2020, **60**, 345-350.
4. Y. Guo, T. Wang, Q. Yang, X. Li, H. Li, Y. Wang, T. Jiao, Z. Huang, B. Dong, W. Zhang, J. Fan and C. Zhi, *ACS Nano*, 2020, **14**, 9089-9097.
5. J. Lan, M. Peng, P. Liu, D. Chen, X. Xu, M. Luo, Y. Tan and M. Chen, *Mater. Today*, 2020, **38**, 58-66.
6. W. Qiu, N. Yang, D. Luo, J. Wang, L. Zheng, Y. Zhu, E. M. Akinoglu, Q. Huang, L. Shui, R. Wang, G. Zhou, X. Wang and Z. Chen, *Appl. Catal. B: Environ.*, 2021, **293**, 120216.
7. J. Zhang, Y. Ji, P. Wang, Q. Shao, Y. Li and X. Huang, *Adv. Funct. Mater.*, 2019, **30**, 1906579.
8. J. Wang, B. Huang, Y. Ji, M. Sun, T. Wu, R. Yin, X. Zhu, Y. Li, Q. Shao and X. Huang, *Adv. Mater.*, 2020, **32**, e1907112.
9. J. Chen, Y. Kang, W. Zhang, Z. Zhang, Y. Chen, Y. Yang, L. Duan, Y. Li and W. Li, *Angew. Chem. Int. Ed. Engl.*, 2022, e202203022.

10. T. Wu, H. Zhao, X. Zhu, Z. Xing, Q. Liu, T. Liu, S. Gao, S. Lu, G. Chen, A. M. Asiri, Y. Zhang and X. Sun, *Adv. Mater.*, 2020, **32**, e2000299.

11. M.-M. Shi, D. Bao, S.-J. Li, B.-R. Wulan, J.-M. Yan and Q. Jiang, *Adv. Energy Mater.*, 2018, **8**, 1800124.

12. W. Peng, M. Luo, X. Xu, K. Jiang, M. Peng, D. Chen, T. S. Chan and Y. Tan, *Adv. Energy Mater.*, 2020, **10**, 2001364.

13. X. Zhu, J. Zhao, L. Ji, T. Wu, T. Wang, S. Gao, A. A. Alshehri, K. A. Alzahrani, Y. Luo, Y. Xiang, B. Zheng and X. Sun, *Nano Res.*, 2019, **13**, 209-214.

14. H.-B. Wang, J.-Q. Wang, R. Zhang, C.-Q. Cheng, K.-W. Qiu, Y.-J. Yang, J. Mao, H. Liu, M. Du, C.-K. Dong and X.-W. Du, *ACS Catal.*, 2020, **10**, 4914-4921.

15. N. C. Kani, A. Prajapati, B. A. Collins, J. D. Goodpaster and M. R. Singh, *ACS Catal.*, 2020, **10**, 14592-14603.

16. J. Li, S. Chen, F. Quan, G. Zhan, F. Jia, Z. Ai and L. Zhang, *Chem*, 2020, **6**, 885-901.

17. X. Wei, M. Pu, Y. Jin and M. Wessling, *ACS Appl. Mater. Inter.*, 2021, **13**, 21411-21425.

18. S. Hao, M. Liu, J. Pan, X. Liu, X. Tan, N. Xu, Y. He, L. Lei, X. Zhang, Nat. Commun., 2020, 11, 5368.